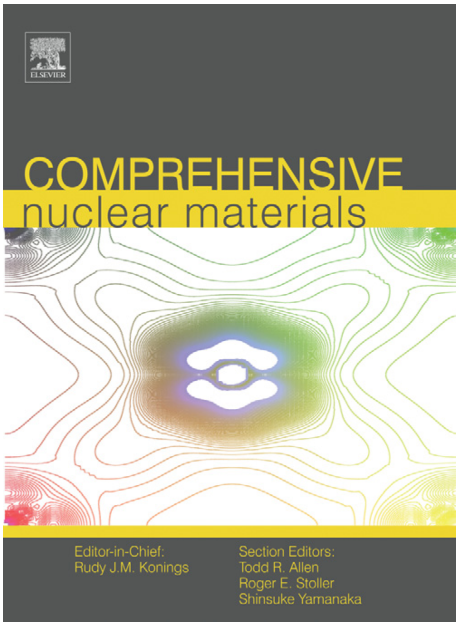

Cai W., Li J., and Yip S. (2012) Molecular Dynamics. In: Konings R.J.M., (ed.) Comprehensive Nuclear Materials, volume 1, pp. 249-265 Amsterdam: Elsevier.

1.09 Molecular Dynamics

W. Cai
Stanford University, Stanford, CA, USA
J. Li
University of Pennsylvania, Philadelphia, PA, USA
S. Yip
Massachusetts Institute of Technology, Cambridge, MA, USA

Abbreviations

bcc Body-centered cubic structure
CSD Central symmetry deviation
EAM Embedded Atom Method potential
FS Finnis–Sinclair potential
MD Molecular dynamics simulation
NMR Nuclear Magnetic Resonance experiment
nn Nearest-neighbor distance
NPT Ensemble in which number of atoms, pressure and temperature are constant
NVE Ensemble in which number of atoms, volume and total energy are constant
NVT Ensemble in which number of atoms, volume and temperature are constant
PBC Periodic boundary condition

1.09.1 Introduction

A concept that is fundamental to the foundations of *Comprehensive Nuclear Materials* is that of microstructural evolution in extreme environments. Given the current interest in nuclear energy, an emphasis on how defects in materials evolve under conditions of high temperature, stress, chemical reactivity, and radiation field presents tremendous scientific and technological challenges, as well as opportunities, across the many relevant disciplines in this important undertaking of our society. In the emerging field of computational science, which may simply be defined as the use of advanced computational capabilities to solve complex problems, the collective contents of *Comprehensive Nuclear Materials* constitute a set of compelling and specific materials problems that can benefit from science-based solutions, a situation that is becoming increasingly recognized.[1–4] In discussions among communities that share fundamental scientific capabilities and bottlenecks, multiscale modeling and simulation is receiving attention for its ability to elucidate the underlying mechanisms governing the materials phenomena that are critical to nuclear fission and fusion applications. As illustrated in Figure 1, molecular dynamics (MD) is an atomistic simulation method that can provide details of atomistic processes in microstructural evolution.

As the method is applicable to a certain range of length and time scales, it needs to be integrated with other computational methods to span the length and time scales of interest to nuclear materials.[9]

The aim of this chapter is to discuss in elementary terms the key attributes of MD as a principal method of studying the evolution of an assembly of atoms under well-controlled conditions. The introductory section is intended to be helpful to students and nonspecialists. We begin with a definition of MD, followed by a description of the ingredients that go into the simulation, the properties that one can calculate with this approach, and the reasons why the method is unique in computational materials research. We next examine results of case studies obtained using an open-source code to illustrate how one can study the structure and elastic properties of a perfect crystal in equilibrium and the mobility of an edge dislocation. We then return to Figure 1 to provide a perspective on the potential as well as the limitations of MD in multiscale materials modeling and simulation.

1.09.2 Defining Classical MD Simulation Method

In the simplest physical terms, MD may be characterized as a method of 'particle tracking.' Operationally, it is a method for generating the trajectories of a system of N particles by direct numerical integration of Newton's equations of motion, with appropriate specification of an interatomic potential and suitable initial and boundary conditions. MD is an atomistic modeling and simulation method when the particles in question are the atoms that constitute the material of interest. The underlying assumption is that one can treat the ions and electrons as a single, classical entity. When this is no longer a reasonable approximation, one needs to consider both ion and electron motions. One can then distinguish two versions of MD, classical and *ab initio*, the former for treating atoms as classical entities (position and momentum) and the latter for treating separately the electronic and ionic degrees of freedom, where a wave function description is used for the electrons. In this chapter, we are concerned only with classical MD. The use of *ab initio* methods in nuclear materials research is addressed elsewhere (**Chapter 1.08, *Ab Initio* Electronic Structure Calculations for Nuclear Materials**). Figure 2 illustrates the MD simulation system as a collection of N particles contained in a volume Ω. At any instant of time t, the particle coordinates are labeled as a $3N$-dimensional vector, $\mathbf{r}^{3N}(t) \equiv \{\mathbf{r}_1(t), \mathbf{r}_2(t), \ldots, \mathbf{r}_N(t)\}$, where $\mathbf{r}_i$ represents the three coordinates of atom i. The simulation proceeds with the system in a prescribed initial configuration, $\mathbf{r}^{3N}(t_0)$, and velocity, $\dot{\mathbf{r}}^{3N}(t_0)$, at time $t = t_0$. As the simulation proceeds, the particles evolve through a sequence of time steps, $\mathbf{r}^{3N}(t_0) \to \mathbf{r}^{3N}(t_1) \to \mathbf{r}^{3N}(t_2) \to \cdots \to \mathbf{r}^{3N}(t_L)$, where $t_k = t_0 + k\Delta t$, $k = 1, 2, \ldots, L$, and Δt is the time step of MD simulation. The simulation runs for L number of steps and covers a time interval of $L\Delta t$. Typical values of L can range from 10^4 to 10^8 and $\Delta t \sim 10^{-15}$s. Thus, nominal MD simulations follow the system evolution over time intervals not more than ~1–10 ns.

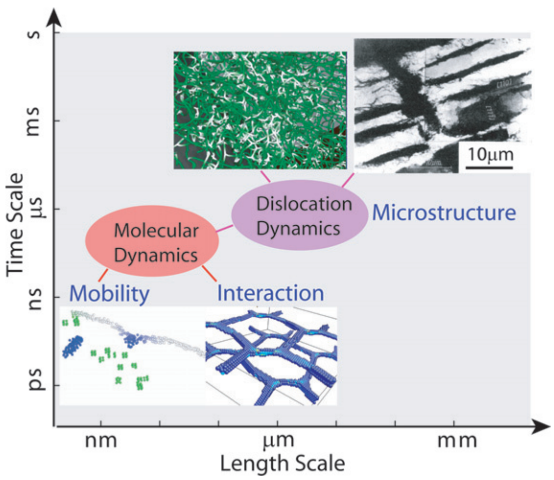

Figure 1 MD in the multiscale modeling framework of dislocation microstructure evolution. The experimental micrograph shows dislocation cell structures in Molybdenum.[5] The other images are snapshots from computer models of dislocations.[6–8]

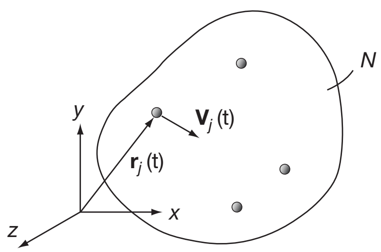

Figure 2 MD simulation cell is a system of N particles with specified initial and boundary conditions. The output of the simulation consists of the set of atomic coordinates $\mathbf{r}^{3N}$(t) and corresponding velocities (time derivatives). All properties of the MD simulation are then derived from the trajectories, $\{\mathbf{r}^{3N}(t), \dot{\mathbf{r}}^{3N}(t)\}$.

The simulation system has a certain energy E, the sum of the kinetic and potential energies of the particles, $E = K + U$, where K is the sum of individual kinetic energies

$$K = \frac{1}{2}m\sum_{j=1}^{N}\mathbf{v}_j \cdot \mathbf{v}_j \qquad [1]$$

and $U = U(\mathbf{r}^{3N})$ is a prescribed interatomic interaction potential. Here, for simplicity, we assume that all particles have the same mass m. In principle, the potential U is a function of all the particle coordinates in the system if we allow each particle to interact with all the others without restriction. Thus, the dependence of U on the particle coordinates can be as complicated as the system under study demands. However, for the present discussion we introduce an approximation, the assumption of a two-body or pair-wise additive interaction, which is sufficient to illustrate the essence of MD simulation.

To find the atomic trajectories in the classical version of MD, one solves the equations governing the particle coordinates, Newton's equations of motion in mechanics. For our N-particle system with potential energy U, the equations are

$$m\frac{\mathrm{d}^2\mathbf{r}_j}{\mathrm{d}t^2} = -\nabla_{\mathbf{r}_j}U(\mathbf{r}^{3N}), j = 1, \ldots, N \qquad [2]$$

where m is the particle mass. Equation [2] may look deceptively simple; actually, it is as complicated as the famous N-body problem that one generally cannot solve exactly when N is >2. As a system of coupled second-order, nonlinear ordinary differential equations, eqn [2] can be solved numerically, which is what is carried out in MD simulation.

Equation [2] describes how the system (particle coordinates) evolves over a time period from a given initial state. Suppose we divide the time period of interest into many small segments, each being a time step of size Δt. Given the system conditions at some initial time t_0, $\mathbf{r}^{3N}(t_0)$, and $\dot{\mathbf{r}}^{3N}(t_0)$, integration means we advance the system successively by increments of Δt,

$$\mathbf{r}^{3N}(t_0) \to \mathbf{r}^{3N}(t_1) \to \mathbf{r}^{3N}(t_2) \to \cdots \to \mathbf{r}^{3N}(t_L) \qquad [3]$$

where L is the number of time steps making up the interval of integration.

How do we numerically integrate eqn [3] for a given U? A simple way is to write a Taylor series expansion,

$$\mathbf{r}_j(t_0 + \Delta t) = \mathbf{r}_j(t_0) + \mathbf{v}_j(t_0)\Delta t + 1/2\mathbf{a}_j(t_0)(\Delta t)^2 + \cdots \qquad [4]$$

and a similar expansion for $\mathbf{r}_j(t_0 - \Delta t)$. Adding the two expansions gives

$$\mathbf{r}_j(t_0 + \Delta t) = -\mathbf{r}_j(t_0 - \Delta t) + 2\mathbf{r}_j(t_0) + \mathbf{a}_j(t_0)(\Delta t)^2 + \cdots \qquad [5]$$

Notice that the left-hand side of eqn [5] is what we want, namely, the position of particle j at the next time step $t_0 + \Delta t$. We already know the positions at t_0 and the time step before, so to use eqn [5] we need the acceleration of particle j at time t_0. For this we substitute $\mathbf{F}_j(\mathbf{r}^{3N}(t_0))/m$ in place of acceleration $\mathbf{a}_j(t_0)$, where $\mathbf{F}_j$ is just the right-hand side of eqn [2]. Thus, the integration of Newton's equations of motion is accomplished in successive time increments by applying eqn [5]. In this sense, MD can be regarded as a method of particle tracking where one follows the system evolution in discrete time steps. Although there are more elaborate, and therefore more accurate, integration procedures, it is important to note that MD results are as rigorous as classical mechanics based on the prescribed interatomic potential. The particular procedure just described is called the Verlet (leapfrog)[10] method. It is a symplectic integrator that respects the symplectic symmetry of the Hamiltonian dynamics; that is, in the absence of floating-point round-off errors, the discrete mapping rigorously preserves the phase space volume.[11,12] Symplectic integrators have the advantage of long-term stability and usually allow the use of larger time steps than nonsymplectic integrators. However, this advantage may disappear when the dynamics is not strictly Hamiltonian, such as when some thermostating procedure is applied. A popular time integrator used in many early MD codes is the Gear predictor–corrector method[13] (nonsymplectic) of order 5. Higher accuracy of integration allows one to take a larger value of Δt so as to cover a longer time interval for the same number of time steps. On the other hand, the trade-off is that one needs more computer memory relative to the simpler method.

A typical flowchart for an MD code[11] would look something like **Figure 3**. Among these steps, the part that is the most computationally demanding is the force calculation. The efficiency of an MD simulation therefore depends on performing the force calculation as simply as possible without compromising the physical description (simulation fidelity). Since the force is calculated by taking the gradient of the potential U, the specification of U essentially determines the compromise between physical fidelity and computational efficiency.

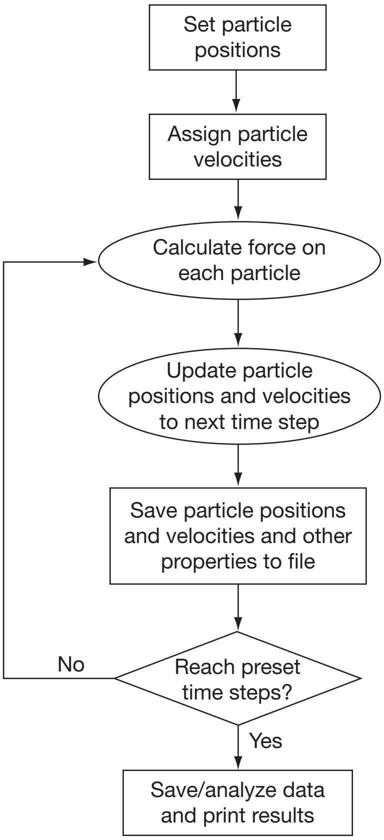

Figure 3 Flow chart of MD simulation.

1.09.3 The Interatomic Potential

This is a large and open-ended topic with an extensive literature.[14] It is clear from eqn [2] that the interaction potential is the most critical quantity in MD modeling and simulation; it essentially controls the numerical and algorithmic simplicity (or complexity) of MD simulation and, therefore, the physical fidelity of the simulation results. Since **Chapter 1.10, Interatomic Potential Development** is devoted to interatomic potential development, we limit our discussion only to simple classical approximations to $U(\mathbf{r}_1, \mathbf{r}_2, \ldots, \mathbf{r}_N)$.

Practically, all atomistic simulations are based on the Born–Oppenheimer adiabatic approximation, which separates the electronic and nuclear motions.[15] Since electrons move much more quickly because of their smaller mass, during their motion one can treat the nuclei as fixed in instantaneous positions, or equivalently the electron wave functions follow the nuclear motion *adiabatically*. As a result, the electrons are treated as always in their ground state as the nuclei move.

For the nuclear motions, we consider an expansion of U in terms of one-body, two-body, ... N-body interactions:

$$U(\mathbf{r}^{3N}) = \sum_{j=1}^{N} V_1(\mathbf{r}_j) + \sum_{i<j}^{N} V_2(\mathbf{r}_i, \mathbf{r}_j) + \sum_{i<j<k}^{N} V_3(\mathbf{r}_i, \mathbf{r}_j, \mathbf{r}_k) + \cdots \qquad [6]$$

The first term, the sum of one-body interactions, is usually absent unless an external field is present to couple with each atom individually. The second sum is the contribution of pure two-body interactions (pairwise additive). For some problems, this term alone is sufficient to be an approximation to U. The third sum represents pure three-body interactions, and so on.

1.09.3.1 An Empirical Pair Potential Model

A widely adopted model used in many early MD simulations in statistical mechanics is the Lennard-Jones (6-12) potential, which is considered a reasonable description of van der Waals interactions between closed-shell atoms (noble gas elements, Ne, Ar, Kr, and Xe). This model has two parameters that are fixed by fitting to selected experimental data. One should recognize that there is no one single physical property that can determine the entire potential function. Thus, using different data to fix the model parameters of the same potential form can lead to different simulations, making quantitative comparisons ambiguous. To validate a model, it is best to calculate an observable property not used in the fitting and compare with experiment. This would provide a test of the *transferability* of the potential, a measure of robustness of the model. In fitting model parameters, one should use different kinds of properties, for example, an equilibrium or thermodynamic property and a vibrational property to capture the low- and high-frequency responses (the hope is that this would allow a reasonable interpolation over all frequencies). Since there is considerable ambiguity in what is the correct method of fitting potential models, one often has to rely on agreement with experiment as a measure of the goodness of potential. However, this could be misleading unless the relevant physics is built into the model.

For a qualitative understanding of MD essentials, it is sufficient to assume that the interatomic potential U can be represented as the sum of two-body interactions

$$U(\mathbf{r}_1, \ldots, \mathbf{r}_N) \cong \sum_{i<j} V(r_{ij}) \quad [7]$$

where $r_{ij} \equiv |\mathbf{r}_i - \mathbf{r}_j|$ is the separation distance between particles i and j. V is the pairwise additive interaction, a central force potential that is a function of only the scalar separation distance between the two particles, r_{ij}. A two-body interaction energy commonly used in atomistic simulations is the Lennard-Jones potential

$$V(r) = 4\varepsilon[(\sigma/r)^{12} - (\sigma/r)^6] \quad [8]$$

where ε and σ are the potential parameters that set the scales for energy and separation distance, respectively. **Figure 4** shows the interaction energy rising sharply when the particles are close to each other, showing a minimum at intermediate separation and decaying to zero at large distances. The interatomic force

$$F(r) \equiv -\frac{\mathrm{d}V(r)}{\mathrm{d}r} \quad [9]$$

is also sketched in **Figure 4**. The particles repel each other when they are too close, whereas at large separations they attract. The repulsion can be understood as arising from overlap of the electron clouds, whereas the attraction is due to the interaction between the induced dipole in each atom. The value of 12 for the first exponent in $V(r)$ has no special significance, as the repulsive term could just as well be replaced by an exponential. The value of 6 for the second exponent comes from quantum mechanical calculations (the so-called London dispersion force) and therefore is not arbitrary. Regardless of whether one uses eqn [8] or some other interaction potential, a short-range repulsion is necessary to give the system a certain size or *volume* (density), without which the particles will collapse onto each other. A long-range attraction is also necessary for *cohesion* of the system, without which the particles will not stay together as they must in all condensed states of matter. Both are necessary for describing the physical properties of the solids and liquids that we know from everyday experience.

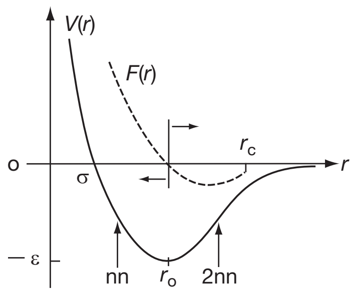

Figure 4 The Lennard–Jones interatomic potential $V(r)$. The potential vanishes at $r = \sigma$ and has a depth equal to $-\varepsilon$. Also shown is the corresponding force $F(r)$ between the two particles (dashed curve), which vanishes at $r_0 = 2^{1/6}\sigma$. At separations less or greater than r_0, the force is repulsive or attractive, respectively. Arrows at nn and 2nn indicate typical separation distances of nearest and second nearest neighbors in a solid.

Pair potentials are simple models that capture the repulsive and attractive interactions between atoms. Unfortunately, relatively few materials, among them the noble gases (He, Ne, Ar, etc.) and ionic crystals (e.g., NaCl), can be well described by pair potentials with reasonable accuracy. For most solid engineering materials, pair potentials do a poor job. For example, all pair potentials predict that the two elastic constants for cubic crystals, C_{12} and C_{44}, must be equal to each other, which is certainly not true for most cubic crystals. Therefore, most potential models for engineering materials include many-body terms for an improved description of the interatomic interaction. For example, the Stillinger–Weber potential[16] for silicon includes a three-body term to stabilize the tetrahedral bond angle in the diamond-cubic structure. A widely used typical potential for metals is the embedded-atom method[17] (EAM), in which the many-body effect is introduced in a so-called embedding function.

1.09.4 Book-keeping Matters

Our simulation system is typically a parallelepiped *supercell* in which particles are placed either in a very regular manner, as in modeling a crystal lattice, or in some random manner, as in modeling a gas or liquid. For the simulation of perfect crystals, the number of particles in the simulation cell can be quite small, and only certain discrete values, such as 256, 500, and 864, should be specified. These numbers pertain to a face-centered-cubic crystal that has four atoms in each unit cell. If our simulation cell has l unit cells along each side, then the number of particles in the cube will be $4l^3$. The above numbers then correspond to cubes with 4, 5, and 6 cells along each side, respectively.

Once we have chosen the number of particles we want to simulate, the next step is to choose the system density we want to study. Choosing the density is equivalent to choosing the system volume since density $\rho = N/\Omega$, where N is the number of particles and Ω is the supercell volume. An advantage of the Lennard-Jones potential is that one can work in dimensionless reduced units. The reduced density $\rho\sigma^3$ has typical values of about 0.9–1.2 for solids and 0.6–0.85 for liquids. For reduced temperature $k_B T/\varepsilon$, the values are $0.4-0.8$ for solids and $0.8-1.3$ for liquids. Notice that assigning particle velocities according to the Maxwellian velocity distribution probability $= (m/2\pi k_B T)^{3/2} \exp[-m(v_x^2+v_y^2+v_z^2)/2k_B T] dv_x\, dv_y\, dv_z$ is tantamount to setting the system temperature T.

For simulation of bulk properties (system with no free surfaces), it is conventional to use the *periodic boundary condition* (PBC). This means that the cubical simulation cell is surrounded by 26 identical image cells. For every particle in the simulation cell, there is a corresponding image particle in each image cell. The 26 image particles move in exactly the same manner as the actual particle, so if the actual particle should happen to move out of the simulation cell, the image particle in the image cell opposite to the exit side will move in and become the actual particle in the simulation cell. The net effect is that particles cannot be lost or created. It follows then that the particle number is conserved, and if the simulation cell volume is not allowed to change, the system density remains constant.

Since in the pair potential approximation, the particles interact two at a time, a procedure is needed to decide which pair to consider among the pairs between actual particles and between actual and image particles. The *minimum image convention* is a procedure in which one takes the nearest neighbor to an actual particle as the interaction partner, regardless of whether this neighbor is an actual particle or an image particle. Another approximation that is useful in keeping the computations to a manageable level is the introduction of a *force cutoff* distance beyond which particle pairs simply do not see each other (indicated as r_c in **Figure 4**). In order to avoid a particle interacting with its own image, it is necessary to set the cutoff distance to be less than half of the simulation cell dimension.

Another book-keeping device often used in MD simulation is a *neighbor list* to keep track of who are the nearest, second nearest, ... neighbors of each particle. This is to save time from checking every particle in the system every time a force calculation is made. The list can be used for several time steps before updating. In low-temperature solids where the particles do not move very much, it is possible to do an entire simulation without, or with only a few, updating, whereas in simulation of liquids, updation every 5 or 10 steps is common.

If one uses a naïve approach in updating the neighbor list (an indiscriminate double loop over all particles), then it will get expensive for more than a few thousand particles because it involves $N \times N$ operations for an N-particle system. For short-range interactions, where the interatomic potential can be safely taken to be zero outside of a cutoff r_c, accelerated approaches exist that can reduce the number of operations from order-N^2 to order-N. For example, in the so-called 'cell lists' approach,[18] one partitions the supercell into many smaller cells, and each cell maintains a registry of the atoms inside (order-N operation). The cell dimension is chosen to be greater than r_c, so an atom cannot possibly interact with more than one neighbor atom. This will reduce the number of operations in updating the neighbor list to order-N.

With the so-called Parrinello–Rahman method,[19] the supercell size and shape can change dynamically during a MD simulation to equilibrate the internal stress with the externally applied constant stress. In these simulations, the supercell is generally nonorthogonal, and it becomes much easier to use the so-called scaled coordinates $\mathbf{s}_j$ to represent particle positions. The scaled coordinates $\mathbf{s}_j$ are related to the real coordinates $\mathbf{r}_j$ through the relation, $\mathbf{r}_j = \mathbf{H} \cdot \mathbf{s}_j$, when both $\mathbf{r}_j$ and $\mathbf{s}_j$ are written as column vectors. $\mathbf{H}$ is a 3×3 matrix whose columns are the three repeat vectors of the simulation cell. Regardless of the shape of the simulation cell, the scaled coordinates of atoms can always be mapped into a unit cube, $[0,1) \times [0,1) \times [0,1)$. The shape change of the simulation cell with time can be accounted for by including the matrix $\mathbf{H}$ into the equation of motion. A 'cell lists' algorithm can still be worked out for a dynamically changing $\mathbf{H}$, which minimizes the number of updates.[13]

For modeling ionic crystals, the long-range electrostatic interactions must be treated differently from short-ranged interactions (covalent, metallic, van der Waals, etc.). This is because a brute-force evaluation of the electrostatic interaction energies involves computation between all ionic pairs, which is of the order N^2, and becomes very time-consuming for large N. The so-called Ewald summation[20,21] decomposes the electrostatic interaction into a short-ranged component, plus a long-ranged component, which, however, can be efficiently summed in the reciprocal space. It reduces the computational time to order $N^{3/2}$. The particle mesh Ewald[22–24] method further reduces the computational time to order $N \log N$.

1.09.5 MD Properties

1.09.5.1 Property Calculations

Let $\langle A \rangle$ denote a time average over the trajectory generated by MD, where A is a dynamical variable, $A(t)$. Two kinds of calculations are of common interest, equilibrium single-point properties and time-correlation functions. The first is a running time average over the MD trajectories

$$\langle A \rangle = \lim_{t\to\infty} \frac{1}{t} \int_o^t dt' A(t') \quad [10]$$

with t taken to be as long as possible. In terms of discrete time steps, eqn [10] becomes

$$\langle A \rangle = \frac{1}{L} \sum_{k=1}^{L} A(t_k) \quad [11]$$

where L is the number of time steps in the trajectory. The second is a time-dependent quantity of the form

$$\langle A(0)B(t) \rangle = \frac{1}{L'} \sum_{k=1}^{L'} A(t_k)B(t_k + t) \quad [12]$$

where B is in general another dynamical variable, and L' is the number of time origins. Equation [12] is called a correlation function of two-dynamical variables; since it is manifestly time dependent, it is able to represent dynamical information of the system.

We give examples of both types of averages by considering the properties commonly calculated in MD simulation.

$$U = \left\langle \sum_{i<j}^{N} V(r_{ij}) \right\rangle \quad \text{potential energy} \quad [13]$$

$$T = \frac{1}{3Nk_B} \left\langle \sum_{i=1}^{N} m_i \mathbf{v}_i \cdot \mathbf{v}_i \right\rangle \quad \text{temperature} \quad [14]$$

$$P = \frac{1}{3\Omega} \left\langle \sum_{i=1}^{N} \left(m_i \mathbf{v}_i \cdot \mathbf{v}_i - \sum_{j>i} \frac{\partial V(r_{ij})}{\partial r_{ij}} r_{ij} \right) \right\rangle \quad \text{pressure} \quad [15]$$

$$g(r) = \frac{1}{\rho 4\pi r^2 N} \left\langle \sum_{i=1}^{N} \sum_{j\neq i} \delta(r - |\mathbf{r}_i - \mathbf{r}_j|) \right\rangle \quad [16]$$

radial distribution function

$$\mathrm{MSD}(t) = \frac{1}{N} \sum_{i=1}^{N} |\mathbf{r}_i(t) - \mathbf{r}_i(0)|^2 \quad [17]$$

mean squared displacement

$$\langle \mathbf{v}(0) \cdot \mathbf{v}(t) \rangle = \frac{1}{N} \sum_{i=1}^{N} \frac{1}{L'} \sum_{k=1}^{L'} \mathbf{v}_i(t_k) \cdot \mathbf{v}_i(t_k + t) \quad [18]$$

velocity autocorrelation function

$$\sigma_{\alpha\beta} = \sum_i \left(\frac{v_a}{\Omega}\right) \sigma^i_{\alpha\beta}, \quad \sigma^i_{\alpha\beta} = \frac{1}{v_a} \left\langle -m v_{i\alpha} v_{i\beta} + \sum_{j>i} \frac{\partial V(r_{ij})}{\partial r_{ij}} \frac{r_{ij\alpha} r_{ij\beta}}{r_{ij}} \right\rangle \quad [19]$$

Virial stress tensor

In eqn [19], v_a is the average volume of one atom, $v_{i\alpha}$ is the α-component of vector $\mathbf{v}_i$, and $r_{ij\alpha}$ is the α-component of vector $\mathbf{r}_i - \mathbf{r}_j$. The interest in writing the stress tensor in the present form is to suggest that the macroscopic tensor can be decomposed into individual atomic contributions, and thus $\sigma^i_{\alpha\beta}$ is known as the atomic level stress[25] at atom i. Although this interpretation is quite appealing, one should be aware that such a decomposition makes sense only in a nearly homogeneous system where every atom 'owns' almost the same volume as every other atom. In an inhomogeneous system, such as in the vicinity of a surface, it is not appropriate to consider such decomposition. Both eqns [15] and [19] are written for pair potential models only. A slightly different expression is required for potentials that contain many-body terms.[26]

1.09.5.2 Properties That Make MD Unique

A great deal can be said about why MD is a useful simulation technique. Perhaps the most important statement is that, in this method, one follows the atomic motions according to the principles of classical mechanics as formulated by Newton and Hamilton. Because of this, the results are physically as meaningful as the potential U that is used. One does not have to apologize for any approximation in treating the N-body problem. Whatever mechanical, thermodynamic, and statistical mechanical properties that a system of N particles should have, they are all present in the simulation data. Of course, how one extracts these properties from the simulation output – the atomic trajectories – determines how useful the simulation is. We can regard MD simulation as an 'atomic video' of the particle motion (which can be displayed as a movie), and how to extract the information in a scientifically meaningful way is up to the viewer. It is to be expected that an experienced viewer can get much more useful information than an inexperienced one.

The above comments aside, we present here the general reasons why MD simulation is useful (or unique). These are meant to guide the thinking of the nonexperts and encourage them to discover and appreciate the many significant aspects of this simulation technique.

(a) *Unified study of all physical properties.* Using MD, one can obtain the thermodynamic, structural, mechanical, dynamic, and transport properties of a system of particles that can be studied in a solid, liquid, or gas. One can even study chemical properties and reactions that are more difficult and will require using quantum MD, or an empirical potential that explicitly models charge transfer.[27]
(b) *Several hundred particles are sufficient to simulate bulk matter.* Although this is not always true, it is rather surprising that one can get quite accurate thermodynamic properties such as equation of state in this way. This is an example that the law of large numbers takes over quickly when one can average over several hundred degrees of freedom.
(c) *Direct link between potential model and physical properties.* This is useful from the standpoint of fundamental understanding of physical matter. It is also very relevant to the structure–property correlation paradigm in material science. This attribute has been noted in various general discussions of the usefulness of atomistic simulations in material research.[28–30]
(d) *Complete control over input, initial and boundary conditions.* This is what provides physical insight into the behavior of complex systems. This is also what makes simulation useful when combined with experiment and theory.
(e) *Detailed atomic trajectories.* This is what one obtains from MD, or other atomistic simulation techniques, that experiment often cannot provide. For example, it is possible to directly compute and observe diffusion mechanisms that otherwise may be only inferred indirectly from experiments. This point alone makes it compelling for the experimentalist to have access to simulation.

We should not leave this discussion without reminding ourselves that there are significant limitations to MD as well. The two most important ones are as follows:

(a) *Need for sufficiently realistic interatomic potential functions U.* This is a matter of what we really know fundamentally about the chemical binding of the system we want to study. Progress is being made in quantum and solid-state chemistry and condensed-matter physics; these advances will make MD more and more useful in understanding and predicting the properties and behavior of physical systems.
(a) *Computational-capability constraints.* No computers will ever be big enough and fast enough. On the other hand, things will keep on improving as far as we can tell. Current limits on how big and how long are a billion atoms and about a microsecond in brute force simulation. A billion-atom MD simulation is already at the micrometer length scale, in which direct experimental observations (such as transmission electron microscopy) are available. Hence, the major challenge in MD simulations is in the time scale, because most of the processes of interest and experimental observations are at or longer than the time scale of a millisecond.

1.09.6 MD Case Studies

In the following section, we present a set of case studies that illustrate the fundamental concepts discussed earlier. The examples are chosen to reflect the application of MD to mechanical properties of crystalline solids and the behavior of defects in them. More detailed discussions of these topics, especially in irradiated materials, can be found in **Chapter 1.11, Primary Radiation Damage Formation** and **Chapter 1.12, Atomic-Level Level Dislocation Dynamics in Irradiated Metals**.

1.09.6.1 Perfect Crystal

Perhaps the most widely used test case for an atomistic simulation program, or for a newly implemented potential model, is the calculation of equilibrium lattice constant a_0, cohesive energy E_{coh}, and bulk modulus B. Because this calculation can be performed using a very small number of atoms, it is also a widely used test case for first-principle simulations (see **Chapter 1.08, *Ab Initio* Electronic Structure Calculations for Nuclear Materials**). Once the equilibrium lattice constants have been determined, we can obtain other elastic constants of the crystal in addition to the bulk modulus. Even though these calculations are not MD *per se*, they are important benchmarks that practitioners usually perform, before embarking on MD simulations of solids. This case study is discussed in **Section 1.09.6.1.1**.

Following the test case at zero temperature, MD simulations can be used to compute the mechanical properties of crystals at finite temperature. Before computing other properties, the equilibrium lattice constant at finite temperature usually needs to be determined first, to account for the thermal expansion effect. This case study is discussed in **Section 1.09.6.1.2**.

1.09.6.1.1 Zero-temperature properties

In this test case, let us consider a body-centered cubic (bcc) crystal of Tantalum (Ta), described by the Finnis–Sinclair (FS) potential.[31] The calculations are performed using the MD++ program. The source code and the input files for this and subsequent test cases in this chapter can be downloaded from http://micro.stanford.edu/wiki/Comprehensive_Nuclear_Materials_MD_Case_Studies.

The cut-off radius of the FS potential for Ta is 4.20 Å. To avoid interaction between an atom with its own periodic images, we consider a cubic simulation cell whose size is much larger than the cut-off radius. The cell dimensions are 5[100], 5[010], and 5[001] along x, y, and z directions, and the cell contains $N = 250$ atoms (because each unit cell of a bcc crystal contains two atoms). PBC are applied in all three directions. The experimental value of the equilibrium lattice constant of Ta is 3.3058 Å. Therefore, to compute the equilibrium lattice constant of this potential model, we vary the lattice constant a from 3.296 to 3.316 Å, in steps of 0.001 Å. The potential energy per atom E as a function of a is plotted in **Figure 5**. The data can be fitted to a parabola. The location of the minimum is the equilibrium lattice constant, $a_0 = 3.3058$ Å. This exactly matches the experimental data because a_0 is one of the fitted parameters of the potential. The energy per atom at a_0 is the cohesive energy, $E_{coh} = -8.100$ eV, which is another fitted parameter. The curvature of parabolic curve at a_0 gives an estimate of the bulk modulus, $B = 197.2$ GPa. However, this is not a very accurate estimate of the bulk modulus because the range of a is still too large. For a more accurate determination of the bulk modulus, we need to compute the $E(a)$ curve again in the range of $|a - a_0| < 10^{-4}$ Å. The curvature of the $E(a)$ curve at a_0 evaluated in the second calculation gives $B = 196.1$ GPa, which is the fitted bulk modulus value of this potential model.[31]

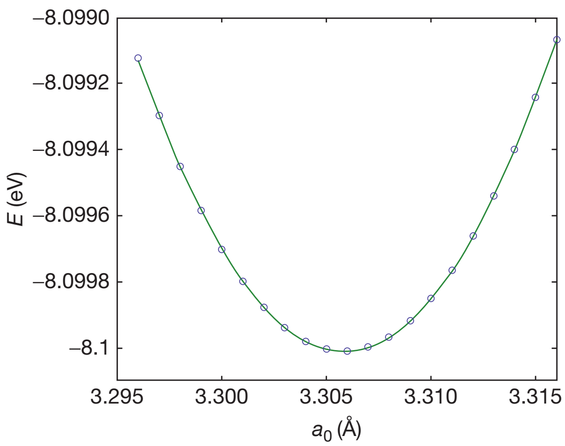

Figure 5 Potential energy per atom as a function of lattice constant of Ta. Circles are data computed from the FS potential, and the line is a parabola fitted to the data.

When the crystal has several competing phases (such as bcc, face-centered cubic, and hexagonal-closed-packed), plotting the energy versus volume (per atom) curves for all the phases on the same graph allows us to determine the most stable phase at zero temperature and zero pressure. It also allows us to predict whether the crystal will undergo a phase transition under pressure.[32]

Other elastic constants besides B can be computed using similar approaches, that is, by imposing a strain on the crystal and monitoring the changes in potential energy. In practice, it is more convenient to extract the elastic constant information from the stress–strain relationship. For cubic crystals, such as Ta considered here, there are only three independent elastic constants, C_{11}, C_{12}, and C_{44}. C_{11} and C_{12} can be obtained by elongating the simulation cell in the x-direction, that is, by changing the cell length into $L = (1 + \varepsilon_{xx}) \cdot L_0$, where $L_0 = 5a_0$ in this test case. This leads to nonzero stress components σ_{xx}, σ_{yy}, σ_{zz}, as computed from the Virial stress formula [19], as shown in **Figure 6** (the atomic velocities are zero because this calculation is quasistatic). The slope of these curves gives two of the elastic constants $C_{11} = 266.0$ GPa and $C_{12} = 161.2$ GPa. These results can be compared with the bulk modulus obtained from potential energy, due to the relation $B = (C_{11} + 2C_{12})/3 = 196.1$GPa.

C_{44} can be obtained by computing the shear stress σ_{xy} caused by a shear strain ε_{xy}. Shear strain ε_{xy} can be applied by adding an off-diagonal element in matrix $\mathbf{H}$ that relates scaled and real coordinates of atoms.

$$\mathbf{H} = \begin{bmatrix} L_0 & 2\varepsilon_{xy} L_0 & 0 \\ 0 & L_0 & 0 \\ 0 & 0 & L_0 \end{bmatrix} \qquad [20]$$

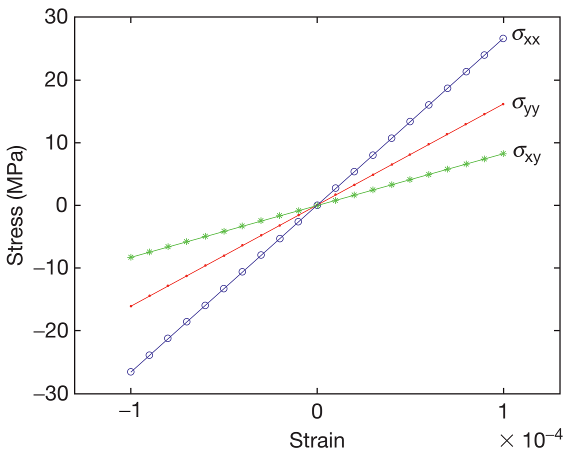

Figure 6 Stress–strain relation for FS Ta: σ_{xx} and σ_{yy} as functions of ε_{xx} and σ_{xy} as a function of ε_{xy}.

The slope of the shear stress–strain curve gives the elastic constant $C_{44} = 82.4$ GPa.

In this test case, all atoms are displaced according to a uniform strain, that is, the scaled coordinates of all atoms remain unchanged. This is correct for simple crystal structures where the basis contains only one atom. For complex crystal structures with more than one basis atom (such as the diamond-cubic structure of silicon), the relative positions of atoms in the basis set will undergo additional adjustments when the crystal is subjected to a macroscopically uniform strain. This effect can be captured by performing energy minimization at each value of the strain before recording the potential energy or the Virial stress values. The resulting 'relaxed' elastic constants correspond well with the experimentally measured values, whereas the 'unrelaxed' elastic constants usually overestimate the experimental values.

1.09.6.1.2 Finite-temperature properties

Starting from the perfect crystal at equilibrium lattice constant a_0, we can assign initial velocities to the atoms and perform MD simulations. In the simplest simulation, no thermostat is introduced to regulate the temperature, and no barostat is introduced to regulate the stress. The simulation then corresponds to the *NVE* ensemble, where the number of particles *N*, the cell volume *V* (as well as shape), and total energy *E* are conserved. This simulation is usually performed as a benchmark to ensure that the numerical integrator is implemented correctly and that the time step is small enough.

The instantaneous temperature T^{inst} is defined in terms of the instantaneous kinetic energy *K* through the relation $K \equiv (3N/2)k_B T^{\text{inst}}$, where k_B is Boltzmann's constant. Therefore, the velocity can be initialized by assigning random numbers to each component of every atom and scaling them so that T^{inst} matches the desired temperature. In practice, T^{inst} is usually set to twice the desired temperature for MD simulations of solids, because approximately half of the kinetic energy flows to the potential energy as the solids reach thermal equilibrium. We also need to subtract appropriate constants from the *x*, *y*, *z* components of the initial velocities to make sure the center-of-mass linear momentum of the entire cell is zero. When the solid contains surfaces and is free to rotate (e.g., a nanoparticle or a nanowire), care must be taken to ensure that the center-of-mass angular momentum is also zero.

Figure 7(a) plots the instantaneous temperature as a function of time, for an MD simulation starting with a perfect crystal and $T^{\text{inst}} = 600$ K, using the Velocity Verlet integrator[13] with a time step of $\Delta t = 1$ fs. After 1 ps, the temperature of the simulation cell is equilibrated around 300 K. Due to the finite time step Δt, the total energy *E*, which should be a conserved quantity in Hamiltonian dynamics, fluctuates during the MD simulation. In this simulation, the total energy fluctuation is $< 2 \times 10^{-4}$ eV per atom, after equilibrium has been reached ($t > 1$ ps). There is also zero long-term drift of the total energy. This is an advantage of symplectic integrators[11,12] and also indicates that the time step is small enough.

The stress of the simulation cell can be computed by averaging the Virial stress for time between 1 and 10 ps. A hydrostatic pressure $P \equiv -(\sigma_{xx} + \sigma_{yy} + \sigma_{zz})/3 = 1.33 \pm 0.01$ GPa is obtained. The compressive stress develops because the crystal is constrained at the zero-temperature lattice constant. A convenient way to find the equilibrium lattice constant at finite temperature is to introduce a barostat to adjust the volume of the simulation cell. It is also convenient to introduce a thermostat to regulate the temperature of the simulation cell. When both the barostat and thermostat are applied, the simulation corresponds to the NPT ensemble.

The Nose–Hoover thermostat[11,33,34] is widely used for MD simulations in NVT and NPT ensembles. However, care must be taken when applying it to perfect crystals at medium-to-low temperatures, in which the interaction between solid atoms is close to harmonic. In this case, the Nose–Hoover thermostat has difficulty in correctly sampling the equilibrium distribution in phase space, as indicated by periodic oscillation of the instantaneous temperature.

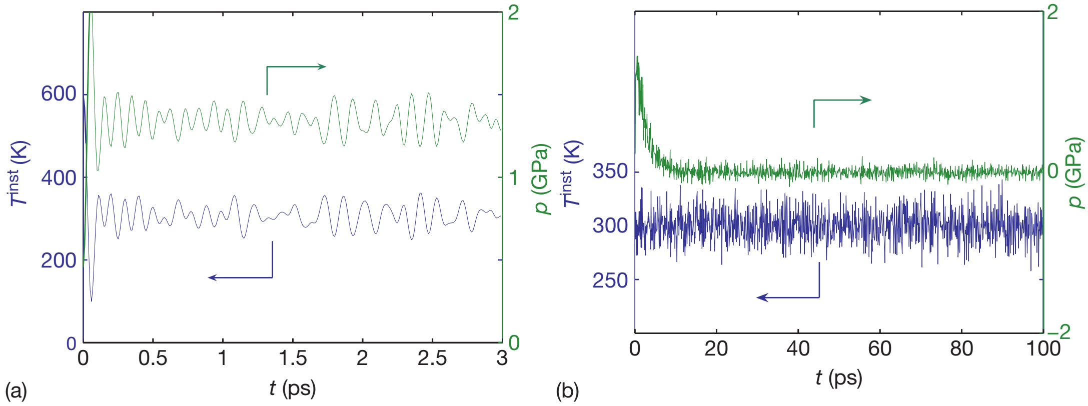

Figure 7 (a) Instantaneous temperature T^{inst} and Virial pressure p as functions of time in an *NVE* simulation with initial temperature at 600 K. (b) T^{inst} and P in a series of NVT at $T = 300$ K, where the simulation cell length L is adjusted according to the averaged value of P.

The Nose–Hoover chain[35] method has been developed to address this problem.

The Parrinello–Rahman[19] method is a widely used barostat for MD simulations. However, periodic oscillations in box size are usually observed during equilibration of solids. This oscillation can take a very long time to die out, requiring an unreasonably long time to reach equilibrium (after which meaningful data can be collected). A viscous damping term is usually added to the box degree of freedom to accelerate the speed of equilibration. Here, we avoid the problem by performing a series of NVT simulations, each one lasting for 1 ps using the Nose–Hoover chain method with Velocity Verlet integrator and $\Delta t = 1$ fs. Before starting each new simulation, the simulation box is subjected to an additional hydrostatic elastic strain of $\varepsilon = \langle P \rangle / B'$, where $\langle P \rangle$ is the average Virial pressure of the previous simulation, where $B' = 2000$GPa is an empirical parameter.

The instantaneous temperature and Virial pressure during 100 of these NVT simulations are plotted in Figure 7(b). The instantaneous temperature fluctuates near the desired temperature (300 K) nearly from the beginning of the simulation. The Virial pressure is well relaxed to zero at $t = 20$ ps. The average box size from 50 to 100 ps is $L = 16.5625$ Å, which is larger than the initial value of 16.5290 Å. This means that the normal strain caused by thermal expansion at 300 K is $\varepsilon_{xx} = 0.00203$. Hence, the coefficient of thermal expansion is estimated to be $\alpha = \varepsilon_{xx}/T = 6.8 \times 10^{-6}\mathrm{K}^{-1}$.[35]

1.09.6.2 Dislocation

Dislocations are line defects in crystals, and their motion is the carrier for plastic deformation of crystals under most conditions ($T < T_m/2$).[36,37] The defects produced by irradiation (such as vacancy and interstitial complexes) interact with dislocations, and this interaction is responsible for the change in the mechanical properties by irradiation (such as embrittlement).[38] MD simulations of dislocation interaction with other defects are discussed in detail in **Chapter 1.12, Atomic-Level Level Dislocation Dynamics in Irradiated Metals**. Here, we describe a more basic case study on the mobility of an edge dislocation in Ta. In Section 1.09.6.2.1, we describe the method of computing its Peierls stress, which is the critical stress to move the dislocation at zero temperature. In Section 1.09.6.2.2, we describe how to compute the mobility of this dislocation at finite temperature by MD.

1.09.6.2.1 Peierls stress at zero temperature

Dislocations in the dominant slip system in bcc metals have $\langle 111 \rangle/2$ Burgers vectors and $\{110\}$ slip planes. Here, we consider an edge dislocation with Burgers vector $\mathbf{b} = 1/2[111]$ (along x-axis), slip plane normal $[\bar{1}10]$ (along y-axis), and line direction $[\bar{1}\,\bar{1}2]$ (along z-axis). To prepare the atomic configuration, we first create a perfect crystal with dimensions $30[111]$, $40[\bar{1}10]$, $2[\bar{1}\,\bar{1}2]$ along the x-, y-, z-axes. We then remove one-fourth of the atomic layers normal to the y-axis to create two free surfaces, as shown in Figure 8(a).

We introduce an edge dislocation dipole into the simulation cell by displacing the positions of all atoms according to the linear elasticity solution of the displacement field of a dislocation dipole. To satisfy PBC, the displacement field is the sum of the contributions from not only the dislocation dipole

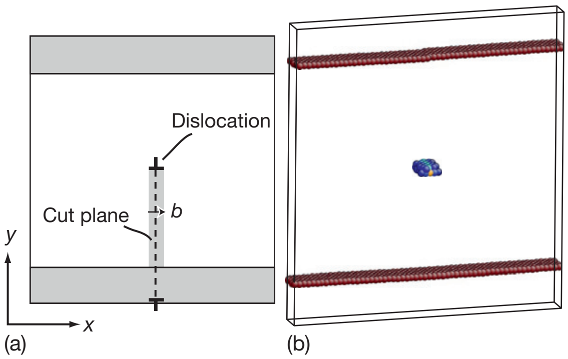

Figure 8 (a) Schematics showing the edge dislocation dipole in the simulation cell. **b** is the dislocation Burgers vector of the upper dislocation. Atoms in shaded regions are removed. (b) Core structure of edge dislocation (at the center) and surface atoms in FS Ta after relaxation visualized by Atomeye.[41] Atoms are colored according to their central-symmetry deviation parameter. Adapted from Li, J. In *Handbook of Materials Modeling*; Yip, S., Ed.; Springer: Dordrecht, 2005; pp 1051–1068; Mistake-free version at http://alum.mit.edu/www/liju99/Papers/05/Li05-2.31.pdf; Kelchner, C. L.; Plimpton, S. J.; Hamilton, J. C. *Phys. Rev. B* **1998**, *58*, 11085.

inside the cell, but also its periodic images. Care must be taken to remove the spurious term caused by the conditional convergence of the sum.[26,40–42] Because the Burgers vector **b** is perpendicular to the cut-plane connecting the two dislocations in the dipole, atoms separated from the cut-plane by $<|\mathbf{b}|/2$ in the x-direction need to be removed. The resulting structure contains 21 414 atoms. The structure is subsequently relaxed to a local energy minimum with zero average stress. Because one of the two dislocations in the dipole is intentionally introduced into the vacuum region, only one dislocation remains after the relaxation, as shown in Figure 8(b).

The dislocation core is identified by central symmetry analysis,[13] which characterizes the degree of inversion-symmetry breaking. In Figure 8(b), only atoms with a central symmetry deviation (CSD) parameter larger than 1.5 Å^2 are plotted. Atoms with CSD parameter between 0.6 and 6 Å^2 appear at the center of the cell and are identified with the dislocation core. Atoms with a CSD parameter between 10 and 20 Å^2 appear at the top and bottom of the cell and are identified with the free surfaces.

The edge dislocation thus created will move along the x-direction when the shear stress σ_{xy} exceeds a critical value. To compute the Peierls stress, we apply shear stress σ_{xy} by adding external forces on surface atoms. The total force on the top surface atoms points in the x-direction and has magnitude of $F_x = \sigma_{xy} L_x L_z$. The total force on the bottom surface atoms has the same magnitude but points in the opposite direction. These forces are equally distributed on the top (and bottom) surface atoms. Because we have removed some atoms when creating the edge dislocation, the bottom surface layer has fewer atoms than the top surface layer. As a result, the external force on each atom on the top surface is slightly lower than that on each atom on the bottom surface.

We apply shear stress σ_{xy} in increments of 1 MPa and relax the structure using the conjugate gradient algorithm at each stress. The dislocation (as identified by the core atoms) does not move for $\sigma_{xy} < 27$ MPa but moves in the x-direction during the relaxation at $\sigma_{xy} = 28$ MPa. Therefore, this simulation predicts that the Peierls stress of edge dislocation in Ta (FS potential) is 28 ± 1 MPa. The Peierls stress computed in this way can depend on the simulation cell size. Therefore, we will need to repeat this calculation for several cell sizes to obtain a more reliable prediction of the Peierls stress. There are other boundary conditions that can be applied to simulate dislocations and compute the Peierls stress, such as PBCs in both x- and y-directions,[42] and the Green's function boundary condition.[44] Different boundary conditions have different size dependence on the numerical error of the Peierls stress.

The simulation cell in this study contains two free surfaces and one dislocation. This is designed to minimize the effect of image forces from the boundary conditions on the computed Peierls stress. If the surfaces were not created, the simulation cell would have to contain at least two dislocations so that the total Burgers vector content was zero. On application of the stress, the two dislocations in the dipole would move in opposite directions, and the total energy would vary as a function of their relative position. This would create forces on the dislocations, in addition to the Peach–Koehler force from the applied stress, and would lead to either overestimation or underestimation of the Peierls stress. On the contrary, the simulation cell described above has only one dislocation, and as it moves to an equivalent lattice site in the x-direction, the energy does not change due to the translational symmetry of the lattice. This means that, by symmetry, the image force on the dislocation from the boundary conditions is identically zero, which leads to more accurate Peierls stress predictions. However, when the simulation cell is too small, the free surfaces in the y-direction and the periodic images in the x-direction can still introduce (second-order) effects on the critical stress for dislocation motion, even though they do not produce any net force on the dislocation.

1.09.6.2.2 Mobility at finite temperature

The relaxed atomic structure from Section 1.09.6.2.1 at zero stress can be used to construct initial conditions for MD simulations for computing dislocation mobility at finite temperature. The dislocation in Section 1.09.6.2.1 is periodic along its length (z-axis) with a relatively short repeat distance ($2[\bar{1}\bar{1}2]$). In a real crystal, the fluctuation of the dislocation line can be important for its mobility. Therefore, we extend the simulation box length by five times along z-axis by replicating the atomic structure before starting the MD simulation. Thus, the MD simulation cell has dimensions $30[111]$, $40[\bar{1}10]$, $10[\bar{1}\bar{1}2]$ along the x, y, z axes, respectively, and contains 10 7070 atoms.

In the following section, we compute the dislocation velocity at several shear stresses at $T = 300$ K. For simplicity, the simulation in which the shear stress is applied is performed under the NVT ensemble. However, the volume of the simulation cell needs to be adjusted from the zero-temperature value to accommodate the thermal expansion effect. The cell dimensions are adjusted by a series of NVT simulations using an approach similar to that used in Section 1.09.6.1.2, except that ε_{xx}, ε_{yy}, ε_{zz} are allowed to adjust independently. As we have found in Section 1.09.6.1.2 that for a perfect crystal, the thermal strain at 300 K is $\varepsilon = 0.00191$, ε_{xx}, ε_{yy}, ε_{zz} are initialized to this value at the beginning of the equilibration.

After the equilibration for 10 ps, we perform MD simulation under different shear stresses σ_{xy} up to 100 MPa. The simulations are performed under the NVT chain method using the Velocity Verlet algorithm with $\Delta t = 1$ fs. The shear stress is applied by adding external forces on surface atoms, in the same way as in Section 1.09.6.2.1. The atomic configurations are saved periodically every 1 ps. For each saved configuration, the CSD parameter[45] of each atom is computed. Due to thermal fluctuation, certain atoms in the bulk can also have CSD values exceeding 0.6 Å^2. Therefore, only the atoms whose CSD value is between 4.5 and 10.0 Å^2 are classified as dislocation core atoms.

Figure 9(a) plots the average position $\langle x \rangle$ of dislocation core atoms as a function of time at different applied stresses. Due to PBC in x-direction, it is possible to have certain core atoms at the left edge of the cell with other core atoms at the right edge of the cell, when the dislocation core moves to the cell border. In this case, we need to ensure that all atoms are within the nearest image of one another, when computing their average position in x-direction. When the configurations are saved frequently enough, it is impossible for the dislocation to move by more than the box length in the x-direction since the last time the configuration was saved. Therefore, the average dislocation position $\langle x \rangle$ at a given snapshot is taken to be the nearest image of the average dislocation position at the previous snapshot so that the $\langle x \rangle(t)$ plots in Figure 9(a) appear as smooth curves.

Figure 9(a) shows that all the $\langle x \rangle(t)$ curves at $t = 0$ have zero slope and nonzero curvature,

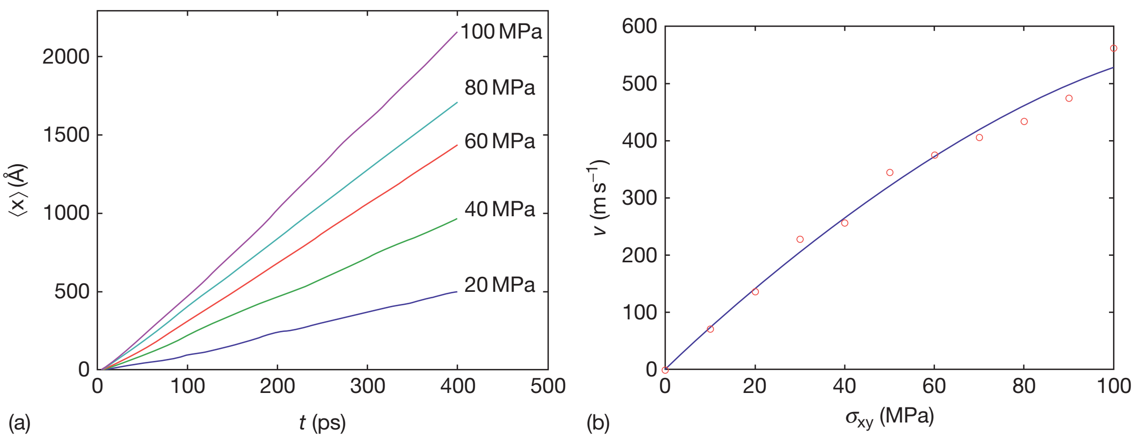

Figure 9 (a) Average position of dislocation core atoms as a function of time at different shear stresses. (b) Dislocation velocity as a function of σ_{xy} at $T = 300$ K.

indicating that the dislocation is accelerating. Eventually, $\langle x \rangle$ becomes a linear function of t, indicating that the dislocation has settled down into steady-state motion. The dislocation velocity is computed from the slope of the $\langle x \rangle(t)$ in the second half of the time period. **Figure 9(b)** plots the dislocation velocity obtained in this way as a function of the applied shear stress. The dislocation velocity appears to be a linear function of stress in the low stress limit, with mobility $M = v/(\sigma_{xy} \cdot b) = 2.6 \times 10^4\,\mathrm{Pa}^{-1}\,\mathrm{s}^{-1}$. Dislocation mobility is one of the important material input parameters to dislocation dynamics (DD) simulations.[46–48]

For accurate predictions of the dislocation velocity and mobility, MD simulations must be performed for a long enough time to ensure that steady-state dislocation motion is observed. The simulation cell size also needs to be varied to ensure that the results have converged to the large cell limit. For large simulation cells, parallel computing is usually necessary to speed up the simulation. The LAMMPS program[49] (http://lammps.sandia.gov) developed at Sandia National Labs is a parallel simulation program that has been widely used for MD simulations of solids.

1.09.7 Perspective

The previous sections give a hands-on introduction to the basic techniques of MD simulation. More involved discussions of the technical aspects may be found in the literature.[30] Here, we offer comments on several enduring attributes of MD from the standpoint of benefits and drawbacks, along with an outlook on future development.

MD has an unrivalled ability for describing material geometry, that is, structure. The Greek philosopher Democritus (ca. 460 BCE–370 BCE) recognized early on that the richness of our world arose from an assembly of atoms. Even without very sophisticated interatomic potentials, a short MD simulation run will place atoms in quite 'reasonable' locations with respect to each other so that their cores do not overlap. This does not mean that the atomic positions are correct, as there could be multiple metastable configurations, but it provides reasonable guesses. Unlike some other simulation approaches, MD is capable of offering real geometric surprises, that is to say, providing new structures that the modeler would never have expected before the simulation run. For this reason, visualization of atomistic structure at different levels of abstraction is very important, and there are several pieces of free software for this purpose.[13,50,51]

As the ball-and-stick model of DNA by Watson and Crick[52] was nothing but an educated guess based on atomic radii and bond angles, MD simulations can be regarded as 'computational Watson and Crick' that are potentially powerful for structural discovery. This remarkable power is both a blessing and a curse for modelers, depending on how it is harnessed. Remember that Watson and Crick had X-ray diffraction data against which to check their structural model. Therefore, it is very important to check the MD-obtained structures against experiments (diffraction, high-resolution transmission electron microscopy, NMR, etc.) and *ab initio* calculations whenever one can.

Another notable allure of MD simulations is that it creates a 'perfect world' that is internally consistent, and all the information about this world is accessible. If MD simulation is regarded as a numerical experiment, it is quite different from real experiments, which all practitioners know are 'messy' and involve extrinsic factors. Many of these extrinsic factors may not be well controlled, or even properly identified, for instance, moisture in the carrier gas, initial condition of the sample, the effects of vibration, thermal drift, and so on. The MD 'world' is much smaller, with perfectly controlled initial conditions and boundary conditions. In addition, real experiments can only probe a certain aspect, a small subset of the properties, while MD simulation gives the complete information. When the experimental result does not work out as expected, there could be extraneous factors, such as a vacuum leak, impurity in the reagents, and so on that could be very difficult to trace back. In contrast, when a simulation gives a result that is unexpected, there is always a way to understand it, because one has complete control of the initial conditions, boundary conditions, and all the intermediate configurations. One also has access to the code itself. A simulation, even if a wrong one (with bugs in the program), is always repeatable. Not so with actual experiments.

It is certainly true that any interatomic potential used in an MD simulation has limitations, which means the simulation is always an approximation of the real material. It also can happen that the limitations are not as serious as one might think, such as in establishing a conceptual framework for fundamental mechanistic studies. This is because the value of MD is much greater than simply calculating material parameters. MD results can contribute a great deal towards constructing a conceptual framework and some kind of analytical model. Once the conceptual framework and analytical model are established, the parameters for a specific material may be obtained by more accurate *ab initio* calculations or more readily by experiments. It would be bad practice to regard MD simulation primarily as a black box that can provide a specific value for some property, without a deeper analysis of the trajectories and interpretation in light of an appropriate framework. Such a framework, external to the MD simulation, is often broadly applicable to a variety of materials; for example, the theory and expressions of solute strengthening in alloys based on segregation in the dislocation core. If solute strengthening occurs in a wide variety of materials, then it should also occur in 'computer materials.' Indeed, the ability to parametrically tune the interatomic potential, to see which energetic aspect is more important for a specific behavior or property, is a unique strength of MD simulations compared with experiments. One might indeed argue that the value of science is to reduce the complex world to simpler, easier-to-process models. If one wants only all the unadulterated complexity, one can just look at the world without doing anything. Thus, the main value of simulation should not be in the *final result* but also in the *process*, and the role of simulations should be to help simplify and clarify, not just to reproduce, the complexity. According to this view, the problem with a specific interatomic potential is not that it does not work, but that it is not known which properties the potential can describe and which it cannot, and why.

There are also fundamental limitations in the MD simulation method that deserve comment. The algorithm is entirely classical, that is, it is Newtonian mechanics. As such, it misses relativistic and quantum effects. Below the Debye temperature,[53] quantum effects become important. The equipartition theorem from classical statistical mechanics, stating that every degree of freedom possesses $k_B T/2$ kinetic energy, breaks down for the high-frequency modes at low temperatures. In addition to thermal uncertainties in a particle's position and momentum, there are also superimposed quantum uncertainties (fluctuations), reflected by the zero-point motion. These effects are particularly severe for light-mass elements such as hydrogen.[54] There exist rigorous treatments for mapping the equilibrium thermodynamics of a quantum system to a classical dynamics system. For instance, path-integral molecular dynamics (PIMD)[55,56] can be used to map each quantum particle to a ring of identical classical particles connected by Planck's constant-dependent springs to represent quantum fluctuations (the 'multi-instance' classical MD approach). There are also approaches that correct for the quantum heat capacity effect with single-instance MD.[53,57] For quantum dynamical properties outside of thermal equilibrium, or even for evaluating equilibrium time-correlation functions, the treatment based on an MD-like algorithm becomes even more complex.[58–60]

It is well recognized in computational material research that MD has a time-scale limitation. Unlike viscous relaxation approaches that are first order in time, MD is governed by Newtonian dynamics that is second order in time. As such, inertia and vibration are essential features of MD simulation. The necessity to resolve atomic-level vibrations requires the MD time step to be of the order picosecond/100, where a picosecond is the characteristic time period for the highest-frequency oscillation mode in typical materials, and about 100 steps are needed to resolve a full oscillation period with sufficient accuracy. This means that the typical timescale of MD simulation is at the nanosecond level, although with massively parallel computer and linear-scaling parallel programs such as LAMMPS,[49] one may push the simulations to microsecond to millisecond level nowadays. A nanosecond-level MD simulation is often enough for the convergence of physical properties such as elastic constants, thermal expansion, free energy, thermal conductivity, and so on. However, chemical reaction processes, diffusion, and mechanical behavior often depend on events that are 'rare' (seen at the level of atomic vibrations) but important, for instance, the emission of a dislocation from grain boundary or surface.[61] There is no need to track atomic vibrations, important as they are, for time periods much longer than a nanosecond for any particular atomic configuration. Important conceptual and algorithmic advances were made in the so-called Accelerated Molecular Dynamics approaches,[62–66] which filter out repetitive vibrations and are expected to become more widely used in the coming years.

> ... Above all, it seems to me that the human mind sees only what it expects.

These are the words of Emilio Segré (Noble Prize in Physics, 1959, for the discovery of the antiproton) in a historical account of the discovery of nuclear fission by O. Hahn and F. Strassmann,[67] which led to a Nobel Prize in Chemistry, 1944, for Hahn. Prior to the discovery, many well-known scientists had worked on the problem of bombarding uranium with neutrons, including Fermi in Rome, Curie in Paris, and Hahn and Meitner in Berlin. All were looking for the production of transuranic elements (elements heavier than uranium), and none were open minded enough to recognize the fission reaction. As atomistic simulation can be regarded as an 'atomic camera,' it would be wise for anyone who wishes to study nature through modeling and simulation to keep an open mind when interpreting simulation results.

Acknowledgments

W. Cai appreciates the assistance from Keonwook Kang and Seunghwa Ryu in constructing the case studies and acknowledges support by NSF grant CMS-0547681, AFOSR grant FA9550-07-1-0464, and the Army High Performance Computing Research Center at Stanford. J. Li acknowledges support by NSF grant CMMI-0728069 and DMR-1008104, MRSEC grant DMR-0520020, and AFOSR grant FA9550-08-1-0325.

References

1. Guérin, Y.; Was, G. S.; Zinkle, S. J. *MRS Bull.* **2009**, *34*(1), 10–19.
2. *Basic Research Needs for Advanced Nuclear Energy Systems: Report of the Basic Energy Sciences Workshop on Basic Research Needs for Advanced Nuclear Energy Systems*; U.S. Department of Energy Office of Basic Energy Sciences, 2006.
3. *Simulation Based Engineering Science – Revolutionizing Engineering Science Through Simulation*; National Science Foundation, 2006.
4. *Science Based Nuclear Energy Systems Enabled by Advanced Modeling and Simulation at the Extreme Scale*; U.S. Department of Energy's Offices of Science and Nuclear Energy, 2009.
5. Kopetskii, C. V.; Pashkovskii, A. I. *Phys. Stat. Solidif. A* **1974**, 21.
6. Marian, J.; Cai, W.; Bulatov, V. V. *Nat. Mater.* **2004**, *3*, 158.
7. Bulatov, V. V.; Cai, W. *Phys. Rev. Lett.* **2002**, *89*, 115501.
8. Bulatov, V. V.; Hsiung, L. L.; Tang, M.; *et al. Nature* **2006**, *440*, 1174.
9. *Integrated Computational Materials Engineering: A Transformational Discipline for Improved Competitiveness and National Security*; National Research Council, 2008.
10. Verlet, L. *Phys. Rev.* **1967**, *159*(1), 98–103.
11. Frenkel, D.; Smit, B. *Understanding Molecular Simulation: From Algorithms to Applications*, Academic Press: New York, 2002.
12. Yoshida, H. *Phys. Lett. A* **1990**, *150*(5–7), 262–268.
13. Li, J. In *Handbook of Materials Modeling*; Yip, S., Ed.; Springer, 2005; pp 565–588; Mistake free version at http://alum.mit.edu/www/liju99/Papers/05/Li05-2.8.pdf.
14. Finnis, M. *Interatomic Forces in Condensed Matter*; Oxford University Press: Oxford, 2003.
15. Born, M.; Oppenheimer, R. *Ann. Phys.* **1927**, *84*(20), 457–484.
16. Stillinger, F. H.; Weber, T. A. *Phys. Rev. B* **1985**, *31*, 5262–5271.
17. Daw, M. S.; Baskes, M. I. *Phys. Rev. B* **1984**, *29*, 6443–6453.
18. Allen, M. P.; Tildesley, D. J., *Computer Simulation of Liquids*; Clarendon Press: New York, 1987.
19. Parrinello, M.; Rahman, A. *J. Appl. Phys.* **1981**, *52*(12), 7182–7190.
20. Ewald, P. P. *Ann. Phys.* **1921**, *64*(3), 253–287.
21. de Leeuw, S. W.; Perram, J. W.; Smith, E. R. *Proc. Roy. Soc. Lond. A* **1980**, *373*, 27–56.
22. Darden, T.; York, D.; Pedersen, L. *J. Chem. Phys.* **1993**, *98*, 10089–10093.
23. Essmann, U.; Perera, L.; Berkowitz, M. L.; Darden, T.; Lee, H.; Pedersen, L. G. *J. Chem. Phys.* **1995**, *103*(19), 8577–8593.
24. Deserno, M.; Holm, C. *J. Chem. Phys.* **1998**, *109*(18), 7678–7701.
25. Srolovitz, D.; Vitek, V.; Egami, T. *Acta Metall.* **1983**, *31*(2), 335–352.
26. Bulatov, V. V.; Cai, W. *Computer Simulations of Dislocations*; Oxford University Press: Oxford, 2006.
27. Streitz, F. H.; Mintmire, J. W. *Phys. Rev. B* **1994**, *50*(16), 11996–12003.
28. Yip, S. In *Molecular-Dynamics Simulation of Statistical-Mechanical Systems*; Ciccotti, G.; Hoover, W. G., Eds.; North-Holland: Amsterdam, 1986; pp 523–561.
29. Yip, S. *Nat. Mater.* **2003**, *2*(1), 3–5.
30. Yip, S. *Handbook of Materials Modeling*; Springer: Dordrecht, 2005.
31. Finnis, M. W.; Sinclair, J. E. *Philos. Mag. A Phys.Condens. Matter Struct. Defects Mech. Prop.* **1984**, *50*(1), 45–55.
32. Muller, M.; Erhart, P.; Albe, K. *J. Phys. Condens. Matter* **2007**, *19*(32), 326220–326243.
33. Nose, S. *Mol. Phys.* **1984**, *52*(2), 255–268.
34. Hoover, W. G. *Phys. Rev. A* **1985**, *31*(3), 1695–1697.
35. Martyna, G. J.; Klein, M. L.; Tuckerman, M. *J. Chem. Phys.* **1992**, *97*(4), 2635–2643.
36. Ryu, S.; Cai, W. *Model. Simul. Mater. Sci. Eng.* **2008**, *16*(8), 085005–085017.
37. Frost, H. J.; Ashby, M. F. *Deformation-Mechanism Maps*; Pergamon Press: Oxford, 1982.
38. Hirth, J. P.; Lothe, J. *Theory of Dislocations*; Wiley: New York, 1982; 2nd edn.
39. de la Rubia, T. D.; Zbib, H. M.; Khraishi, T. A.; Wirth, B. D.; Victoria, M.; Caturla, M. J. *Nature* **2000**, *406*(6798), 871–874.
40. Li, J. *Model. Simul. Mater. Sci. Eng.* **2003**, *11*(2), 173–177.
41. Cai, W.; Bulatov, V. V.; Chang, J. P.; Li, J.; Yip, S. *Phys. Rev. Lett.* **2001**, *86*(25), 5727–5730.
42. Cai, W.; Bulatov, V. V.; Chang, J. P.; Li, J.; Yip, S. *Philos. Mag.* **2003**, *83*(5), 539–567.
43. Li, J.; Wang, C. Z.; Chang, J. P.; Cai, W.; Bulatov, V. V.; Ho, K. M.; Yip, S. *Phys. Rev. B* **2004**, *70*(10), 104113–104121.
44. Woodward, C.; Rao, S. *Philos. Mag. A* **2001**, *81*, 1305–1316.
45. Kelchner, C. L.; Plimpton, S. J.; Hamilton, J. C. *Phys. Rev. B* **1998**, *58*, 11085–11088.
46. van der Giessen, E.; Needleman, A. *Model. Simul. Mater. Sci. Eng.* **1995**, *3*, 689–735.
47. Tang, M.; Kubin, L. P.; Canova, G. R. *Acta Mater.* **1998**, *46*, 3221–3235.
48. Cai, W.; Bulatov, V. V.; Chang, J.; Li, J.; Yip, S., In *Dislocations in Solids;* Nabarro, F. R. N.; Hirth, J. P., Eds.; Elsevier: Amsterdam, 2004; Vol. 12, pp 1–80.

49. Plimpton, S. *J. Comput. Phys.* **1995**, *117*(1), 1–19.
50. Bhattarai, D.; Karki, B. B. *J. Mol. Graph.* **2009**, *27*(8), 951–968.
51. Stukowski, A. *Model. Simul. Mater. Sci. Eng*. **2010**, *18*(1), 015012.
52. Watson, J. D.; Crick, F. H. C. *Nature* **1953**, *171*, 737.
53. Li, J.; Porter, L.; Yip, S. *J. Nucl. Mater.* **1998**, *255*(2–3), 139–152.
54. Mills, G.; Jonsson, H.; Schenter, G. K. *Surf. Sci.* **1995**, *324*(2–3), 305–337.
55. Chandler, D.; Wolynes, P. G. *J. Chem. Phys.* **1981**, *74*(7), 4078–4095.
56. Sprik, M. In *Computer Simulation in Materials Science: Interatomic Potentials, Simulation Techniques and Applications*; Meyer, M., Pontikis, V., Eds.; Kluwer: Dordrecht, 1991; pp 305–320.
57. Dammak, H.; Chalopin, Y.; Laroche, M.; Hayoun, M.; Greffet, J. J. *Phys. Rev. Lett.* **2009**, *103*(19), 190601.
58. Jang, S.; Voth, G. A. *J. Chem. Phys.* **1999**, *111*(6), 2357–2370.
59. Miller, W. H. *J. Phys. Chem. A* **2001**, *105*(13), 2942–2955.
60. Poulsen, J. A.; Nyman, G.; Rossky, P. J. *Proc. Natl. Acad. Sci. USA* **2005**, *102*(19), 6709–6714.
61. Zhu, T.; Li, J.; Samanta, A.; Leach, A.; Gall, K. *Phys. Rev. Lett.* **2008**, *100*(2), 025502–025506.
62. Voter, A. F. *Phys. Rev. Lett.* **1997**, *78*(20), 3908–3911.
63. Voter, A. F.; Montalenti, F.; Germann, T. C. *Annu. Rev. Mater. Res.* **2002**, *32*, 321–346.
64. Laio, A.; Parrinello, M. *Proc. Natl. Acad. Sci. USA* **2002**, *99*(20), 12562–12566.
65. Miron, R. A.; Fichthorn, K. A. *J. Chem. Phys.* **2003**, *119*(12), 6210–6216.
66. Hara, S.; Li, J. *Phys. Rev. B* **2010**, *82*(18), 184114–184121.
67. Segre, E. G. *Phys. Today* **1989**, *42*(7), 38–43.